Electronic structure of the Si(111)$\sqrt{3} \times \sqrt{3}R30°$-B surface from theory and photoemission spectroscopy

Hazem Aldahhak,[1,*] Conor Hogan,[2,†] Susi Lindner,[3] Stephan Appelfeller ◉,[3] Holger Eisele,[3] Wolf Gero Schmidt ◉,[1] Mario Dähne,[3] Uwe Gerstmann,[1] and Martin Franz ◉[3,‡]

[1]*Lehrstuhl für Theoretische Materialphysik, Universität Paderborn, 33095 Paderborn, Germany*
[2]*Istituto di Struttura della Materia-CNR (ISM-CNR), Via del Fosso del Cavaliere 100, 00133 Rome, Italy*
[3]*Institut für Festkörperphysik, Technische Universität Berlin, Hardenbergstrasse 36, D-10623 Berlin, Germany*

The Si(111)$\sqrt{3} \times \sqrt{3}R30°$-B [Si(111)-B] surface has evolved into a particularly interesting surface in the context of on-surface molecular self-assembly. Photoemission spectroscopy is a powerful tool to understand the interaction between the surface and the adsorbates. Previous studies of Si(111)-B contain many inconsistencies with regard to the Si 2p core level and valence-band dispersion. Here we employ synchrotron-based core-level and angle-resolved photoemission spectroscopy measurements in combination with density functional theory (DFT) calculations to address these issues. DFT calculations of the Si 2p core-level spectra accurately identify contributions from one bulk and five surface components, which allows us to obtain a comprehensive understanding of the spectra recorded at different photon energies. As an archetypal example, this refined decomposition is employed to understand the changes in Si 2p spectra upon the adsorption of cobalt phthalocyanine molecules. Regarding the valence-band dispersion of the clean Si(111)-B surface, our comprehensive DFT and photoemission investigations are able to reconcile the inconsistencies appearing in previous studies and reveal several yet unreported surface states. Furthermore, we are able to theoretically and experimentally resolve the distribution of these surface states in constant energy plots.

I. INTRODUCTION

The Si(111)$\sqrt{3} \times \sqrt{3}R30°$-B [Si(111)-B] surface has recently attracted considerable attention as a particularly suitable substrate for the growth of organic layers on silicon [1–7]. On common clean silicon surfaces, such as Si(001)2 × 1 or Si(111)7 × 7, the high density of unsaturated dangling bonds typically hinders the ordered growth of organic overlayers. In contrast, these dangling bonds are depopulated on the Si(111)-B surface due to a charge transfer from the adatoms to subsurface B atoms, leading to a passivated surface.

The first observations of the Si(111)-B surface were published in 1988 [8,9]. Its correct structure was identified in 1989 by Headrick *et al.* [10], who used synchrotron x-ray diffraction, and in parallel by Bedrossian *et al.* [11] and Lyo *et al.* [12], who both used a combination of scanning tunneling microscopy (STM) and spectroscopy as well as first-principles calculations. This structure is widely accepted and was later also confirmed and refined by dynamical low-energy electron diffraction [13] and photoelectron diffraction [14]. The corresponding structural model is shown in Fig. 1. The B atoms substitute Si in the second layer in a $\sqrt{3} \times \sqrt{3}R30°$ reconstruction (the so-called S_5 site), while adatoms reside above B atoms in the T_4 position.

Core-level photoemission spectroscopy (PES) and angle-resolved photoemission spectroscopy (ARPES) are key experimental techniques to understand the electronic structure of surfaces and their interaction with adsorbates, e.g., foreign atoms or organic molecules. For the Si(111)-B surface, many works have been published in this context. In particular, the Si 2p core levels are frequently measured and employed to monitor the interactions between the surface and the adsorbates by investigating their energy shifts induced by the adsorbate [6,15–23].

In light of its importance, it is unfortunate that a comprehensive analysis of the Si 2p core-level spectra of Si(111)-B is still missing. For this surface, it is an elusive task to experimentally assign core-level shifts (CLS) to precise chemical environments of the surface atoms. First, the bulk contribution to the measured spectrum is unknown. It is dependent on the kinetic energy of the outgoing photoelectrons [15,18,20,22], but presumably it can be minimized by using photon energies around 130 eV [24]. Second, the Si 2p core level comprises contributions from six chemically inequivalent types of Si atoms (expected to differ by less than 0.65 eV [18,20]) with different relative intensities. Moreover, the contribution of each Si atom type to the total spectrum includes a doublet structure of intensity ratio 2:1 separated by 0.6 eV (spin-orbit splitting). Thus, the overall spectral linewidth will be large compared to the individual contributions of different surface atoms even for an optimum experimental resolution, preventing a clear identification. Third, an explanation of the CLS based on the simple picture of an electron transfer due to

---

*aldahhak@upb.de
†conor.hogan@ism.cnr.it
‡martin.franz@physik.tu-berlin.de
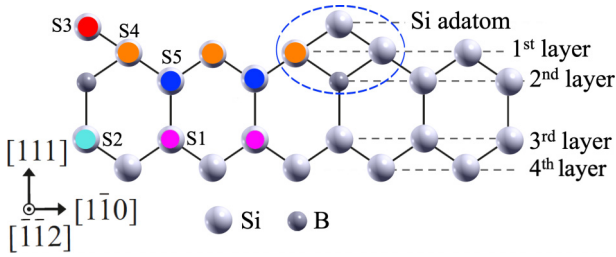
FIG. 1. Schematic sideview of the Si(111)-B surface. The notations for the corresponding surface components in Si $2p$ core-level spectra are denoted (in progressively higher binding energy) as S1–S5. The dashed blue oval indicates the Si adatom and its four nearest neighbors.

bonding with B (note the different electronegativities of Si and B) is not sufficient. There are also other effects, such as the final-state effects related to the question of how strong the positive core hole (produced by photoemission) is screened by the environment. This makes the analysis of the CLS for this surface more difficult and circumvents the characteristic determination of the peak contributions. For such cases, one has to rely on predictive calculations to interpret the experimental data.

Besides core-level spectroscopy, the valence-band dispersion of the Si(111)-B surface has been intensively investigated using ARPES and density functional theory (DFT) [17,19,25–27]. However, several inconsistencies exist among the various ARPES studies. For example, a splitting of the surface-state bands is predicted by theory [27] at both the $\overline{\Gamma}$ and the $\overline{M}$ points. Instead, experimental studies report only either a splitting at $\overline{\Gamma}$ [25] or at $\overline{M}$ [26].

In this paper, we combine both DFT calculations and synchrotron-based PES and ARPES measurements to settle this debate. We decompose the Si $2p$ spectra of Si(111)-B into six (one bulk and five surface) components with accurate ratios. Then, we apply the new decomposition to exemplarily understand the changes in the Si $2p$ spectra upon the adsorption of cobalt phthalocyanine (CoPc) molecules on Si(111)-B. Finally, we perform a comprehensive analysis of the surface electronic structure.

II. METHODOLOGY

A. Theory

DFT calculations were performed with the QUANTUM ESPRESSO package [28]. The Perdew-Burke-Ernzerhof (PBE) exchange-correlation (XC) functional [29] along with the semiempirical Grimme-D3 van der Waals (vdW) correction including Becke-Johnson damping (PBE-D3BJ) [30] were employed to model the electron exchange and correlation. For calculations of CLS, PBE-D2 [31], and local-density approximation (LDA) [32] were also considered. Norm-conserving pseudopotentials were used to describe the electron-ion interactions. Plane waves up to a cutoff energy of 65 Ry were used as basis functions. The Si(111)-B surface was modeled using periodically repeated slabs with a thickness of 8 (core-level) or 14 (band structure) atomic layers separated by 3 nm of vacuum and backterminated by hydrogen.

Supercells of dimensions $\sqrt{3} \times \sqrt{3}$, $2\sqrt{3} \times 2\sqrt{3}$, and $4\sqrt{3} \times 4\sqrt{3}$ with corresponding 4×4, 2×2, and Γ-only k-point meshes were used for calculations of valence-band spectra, core-level shifts, and CoPc adsorption, respectively. Structural optimizations were performed with a tight threshold of 0.25 meV/nm on the atomic forces; the backmost four layers were fixed at their bulk positions. Final optimized geometries were found to be in good agreement with previous DFT-LDA calculations [27] with bond lengths near the surface differing by only 0.002–0.006 nm.

The PES spectra were calculated using a ΔSCF approach [33–35], which allows for the accurate simulation and interpretation of the measured core levels [36–40]. Multiprojector (GI-)projector augmented-wave pseudopotentials [41] with occupation-constrained inner shells were generated to model the core holes. The resulting binding energies (BE) were exclusively shifted to the experimental values. Furthermore, they were superimposed and convoluted with the experimental resolution. We note here that supercells of dimension $2\sqrt{3} \times 2\sqrt{3}$ were used for these calculations in order to minimize the interactions between the holes in the neighboring cells.

B. Sample preparation

To prepare the Si(111)-B samples, heavily p-doped Si(111) wafers (B doped, $< 0.002\ \Omega\,\text{cm}$) obtained from Crystec GmbH, Berlin, were used. They were repeatedly flash annealed to $1200\,^\circ\text{C}$ in ultrahigh vacuum (base pressure 3×10^{-10} mbar) to remove surface contaminations, followed by an annealing step at $950\,^\circ\text{C}$ for 30 min to induce the subsurface B segregation. The samples were heated by direct current, and their temperature was monitored using an infrared pyrometer with an accuracy of $\pm 20\,^\circ\text{C}$. This process results in an atomically smooth and passivated Si(111)-B surface with low defect density.

CoPc molecules were deposited *in situ* by thermal evaporation onto the Si(111)-B substrate kept at room temperature. For this purpose, a home-built effusion cell with a boron nitride crucible and evaporation temperatures of 300–320 $^\circ\text{C}$ were used. The evaporation rate was determined as described in Ref. [6]. During the whole sample preparation, the pressure did not exceed 2×10^{-9} mbar.

C. Photoemission spectroscopy

The PES and ARPES measurements were carried out at room temperature at the UE112 PGM-1 beamline at BESSY II using a SPECS PHOIBOS 100 electron analyzer equipped with a two-dimensional CCD detector. In contrast to previous experimental studies [17,19,25,26,42], this allows a scan of the complete two-dimensional $k_\parallel$ space, resulting in a three-dimensional data set. From this, also constant energy plots can be extracted.

For a quantitative analysis, the spectra were fitted using spin-orbit split doublets with a splitting of 0.60 eV, an intensity ratio of 2:1, and Voigt line profiles for considering both lifetime and instrumental broadening. Both a constant and a Shirley-type background were used. The energy was calibrated using the Fermi edge of a different metallic sample.

TABLE I. (Left) DFT calculated Si $2p$ CLS (in eV) of the Si(111)-B surface using PBE-D3BJ, PBE-D2, and LDA functionals. The different surface components (S1–S5) are referenced to the BE of bulk Si. The relative intensities (Rel. int.) are also given in monolayer (ML). The (+) signs indicate that the related CLS is shifted to higher binding energies. (Right) DFT-guided decomposition of the measured Si $2p$ spectra of clean Si(111)-B for photon energies of $hv = 130$, 160, and 200 eV. The Si types related to the surface components (S1–S5) are defined by color coding in Fig. 1. The BE of each component is referenced to the bulk Si. The BE values are given for the $2p_{3/2}$ components.

Peak	Rel. int. (ML)	DFT functional			$hv = 130$ eV		$hv = 160$ eV		$hv = 200$ eV	
		PBE-D3BJ	PBE-D2	LDA	Rel. int. (ML)	BE (eV)	Rel. int. (ML)	BE (eV)	Rel. int. (ML)	BE (eV)
Bulk Si		0	0	0	0.1	98.68	0.5	98.65	1.2	98.63
S1	$\frac{2}{3}$	+0.03	+0.05	+0.01	$\frac{2}{3}$	+0.02	$\frac{2}{3}$	+0.05	$\frac{2}{3}$	+0.08
S2	$\frac{1}{3}$	+0.12	+0.12	+0.10	0.1	+0.15	$\frac{1}{3}$	+0.17	$\frac{1}{3}$	+0.19
S3	$\frac{1}{3}$	+0.39	+0.38	+0.41	$\frac{1}{3}$	+0.42	$\frac{1}{3}$	+0.41	$\frac{1}{3}$	+0.35
S4	1	+0.40	+0.41	+0.41	1	+0.51	1	+0.48	1	+0.49
S5	$\frac{2}{3}$	+0.52	+0.54	+0.53	$\frac{2}{3}$	+0.58	$\frac{2}{3}$	+0.59	$\frac{2}{3}$	+0.60

III. RESULTS AND DISCUSSIONS

Figure 1 shows a schematic structural model of an ideal (defect free) Si(111)-B surface. Since B atoms occupy the substitutional S_5 site in the second layer, the surface signal is assumed to be dominated by the topmost three or four layers, whereas the bulk signal originates from all atoms underneath [18]. However, our calculations confirm that the CLS of the Si atoms in the fourth atomic layer are shifted by only few meV with respect to bulk Si. Thus, we concentrate on the CLS originating from the first three atomic layers. The structural model of the ideal surface, thus, consists of five different surface components, represented by the color coding in Fig. 1, as well as one bulk component. The real Si(111)-B surface also features defect structures, e.g., B atoms in alternative positions [43] or Si atoms occupying the B sites. The latter are known as Si-Si(S_5) defects and their density depends on the *in situ* annealing conditions during the preparation. In the current samples, however, STM data reveal that these defects have a negligible concentration of about 3% of the adatom density [6,7].

A. Si $2p$ spectra of the clean Si(111)-B surface

Figures 2(b)–2(d) show experimental Si $2p$ spectra measured using photon energies of 130, 160, and 200 eV, comparable with the previous investigations [6,15,25]. Each spectrum consists of a three-peak structure (labeled as P1–P3) situated at BE around 98.7, 99.2, and 99.7 eV, respectively. The intensity of peak P1 increases for higher photon energies, thus, indicating more bulk contributions.

In the literature, many attempts have been undertaken to decompose these spectra into components. In the first core-level spectroscopy study of the clean Si(111)-B surface, McLean *et al.* [15] showed that the Si $2p$ spectrum recorded at a photon energy of 130 eV is dominated by a large contribution from surface overlayers in addition to the signals from bulk Si atoms. Later, Rowe *et al.* [18] suggested that the Si $2p$ core level can be decomposed into one bulk and three surface structures. They denoted the surface structures as S_1–S_3 (for progressively higher BE), where S_1 comprises the adatoms, S_2 includes all the Si atoms in the first, second, and fourth (atomic) layers, whereas S_3 is related to the atoms in the third

atomic layer binding to the B atoms. Some years later, Grehk *et al.* [20] decomposed the Si $2p$ spectrum of Si(111)-B again into one bulk and three surface signals (S_1–S_3) in a way different from that of Rowe *et al.* [18]. Thus, the Si atoms in the second layer plus those in the third layer not binding to the B atoms were assigned to S_1, the Si adatoms plus the whole first layer binding to B are assigned to S_2, whereas S_3 is reported to result from the $\frac{1}{3}$ ML of Si atoms in the third layer binding to the B atoms. Assuming the BE of the bulk as a reference, they reported that the surface signals S_1–S_3 are shifted to higher binding energies by 0.2, 0.4, and 0.65 eV, respectively. However, these assignments were performed heuristically and Grehk *et al.* admitted uncertainties in assigning the S_3 signal [20]. Apart from these experimental investigations, Chang and Stott [44] calculated the CLS of S_5 and T_4 site models [45] of the Si(111)-B surface using a final-state method, being the only theoretical study on Si $2p$ core levels of this surface up to now. The comprehensive theoretical photoemission spectroscopy calculations presented here reveal that these results need, in fact, to be refined.

Our theoretical discussions start by confirming that the calculated Si $2p$ core-level shifts are independent of the choice of vdW correction or XC functional. Table I shows the calculated results using PBE-D3BJ, PBE-D2, and LDA functionals. The essentially identical energetic results confirm the validity of the obtained results.

Besides the bulk component, whose intensity is dependent on the photon energy, five nonequivalent Si types with different intensities have been calculated (S1–S5). The binding energies of these components are shifted to higher values compared to bulk Si (considered as a reference). A corresponding simulated spectrum is shown in Fig. 2(a), not showing the bulk contribution and assuming no attenuation due to the photoelectron mean free path.

Starting from lower to higher binding energies: The S1 (S2) component arises from $\frac{2}{3}$ ML ($\frac{1}{3}$ ML) of Si atoms in the third layer not binding (binding) to B. The first peak (P1) arises, therefore, from the combination of the $p_{3/2}$ structure of the bulk S1 and S2 species, while their $p_{1/2}$ components are responsible for the asymmetric shape of the middle peak (P2). Despite the CLS of S1 and S2 being slightly dependent on the used functional, it is clear that S1 (S2) is shifted by less
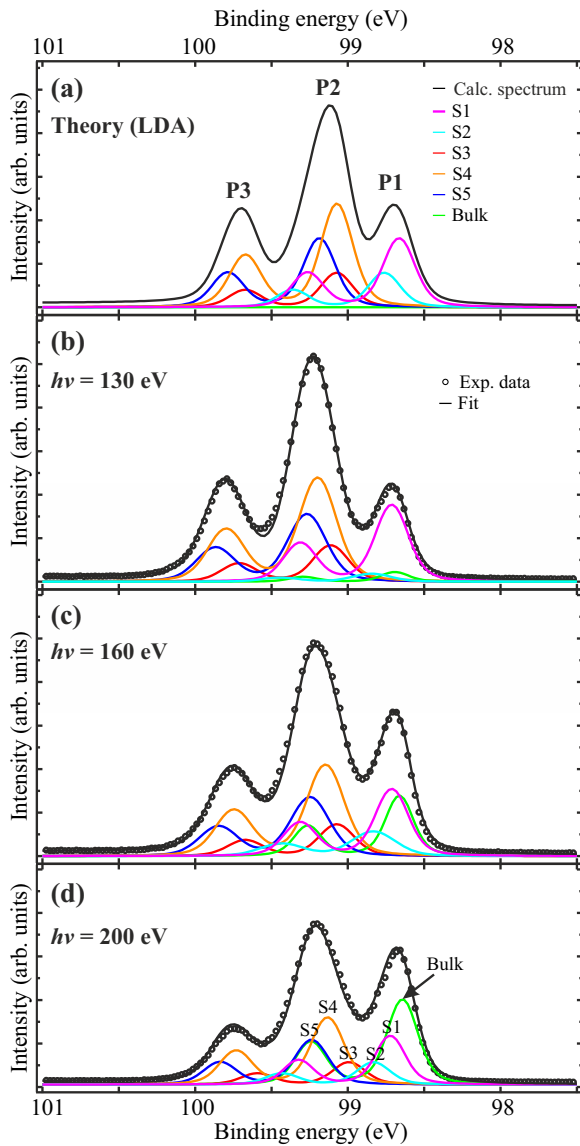
FIG. 2. (a) Calculated Si 2*p* spectrum of Si(111)-B using CLS calculated exemplarily with LDA and assuming only contributions from the surface atoms, i.e., no bulk signal, with Voigt profile broadening similar as used to fit the experimental spectra (i.e., a Lorentzian broadening of 0.085 eV and a Gaussian broadening of 0.2–0.3 eV). The total spectrum, which comprises a three-peak structure (P1–P3), is decomposed into five surface components S1–S5 in ratios of $\frac{2}{3}$ monolayer (ML), $\frac{1}{3}$ ML, $\frac{1}{3}$ ML, 1 ML, and $\frac{2}{3}$ ML, respectively, whereas attenuation effects due to the photoelectron mean free path were not considered. (b)–(d) Experimental Si 2*p* spectra measured using photon energies of (b) $h\nu = 130$ eV, (c) $h\nu = 160$ eV, and (d) $h\nu = 200$ eV. Guided by the calculations, each spectrum is fitted as shown in Table I.

than 50 (150) meV with respect to bulk Si. The fact that S2 has a higher BE compared to S1 (∼100 meV) can be simply explained by the presence of a more electronegative element (B) in the vicinity of the respective Si atoms.

The middle peak (P2) in Fig. 2 arises on one hand from the $p_{3/2}$ structures of the three upper Si types S3–S5, which result from $\frac{1}{3}$ ML of Si adatoms, 1 ML of Si atoms in the first

layer, and $\frac{2}{3}$ ML of Si atoms in the second layer, respectively, but on the other hand also from the $p_{1/2}$ structures of S1 and S2 components as already mentioned. The third peak (P3) in Fig. 2 arises exclusively from the $p_{1/2}$ structures of the S3–S5 components [see the generated spectrum in Fig. 2(a)].

Apparently, this decomposition is critically different from all previously reported investigations. In contrast to, e.g., Grehk *et al.* [20], the two components S1 and S5 are different from each other by about 0.5 eV (they considered them as one component), whereas S2 is shifted with respect to the bulk by about 0.1 eV (they considered it to be shifted by 0.65 eV).

Guided by the DFT results, we decompose the experimental Si 2*p* spectra shown in Figs. 2(b)–2(d) into one bulk and five surface components. Indeed, this decomposition results in excellent fits nicely explaining the spectra for the different photon energies. From the calculated pure surface spectrum shown in Fig. 2(a), it becomes apparent that the measurement with $h\nu = 130$ eV is extremely surface sensitive. At this photon energy, a very low intensity has to be used for the bulk component as well as for the S2 component, which is attenuated more than the S1 component because of the locally thicker overlayer. Thus, the photoemission mainly originates from the topmost three layers. This demonstrates that the measurement really takes place near the minimum of the universal curve [46]. With increasing photon energy, the bulk signal becomes more and more intense [cf. Figs. 2(c) and 2(d)]. The spectra taken with photon energies of 160 and 200 eV can be fitted using exactly the same intensity ratios for the components S1–S5 as in the calculation (here the S2 component is completely taken into account) plus a bulk signal with an intensity corresponding to 0.5 and 1.2 ML for $h\nu = 160$ and $h\nu = 200$ eV, respectively. Note that one should, in principle, consider the mean free path in all experimental spectra and model the intensities of bulk and the "buried" S1 and S2 atoms. But since S1, S2, and bulk Si are very close in energy, this should not affect the general fit results. The energetic positions of the components are also identical for all photon energies and are all consistent with the theoretical results (within the experimental uncertainty). A detailed comparison between the calculated and the experimentally determined CLS is presented in Table I.

The new decomposition of the Si 2*p* core level developed here is not only of importance for the bare surface, but also to understand its interaction with molecules and other adsorbates. For example, Grehk *et al.* [25] observed an extra peak at lower binding energies upon further deposition of Cs on the surface, whereas Fagot-Revurat *et al.* [22] observed exclusive shifts to lower binding energies upon the interaction of K atoms with the topmost surface atoms. In both works, a comprehensive understanding of these changes is missing due to previously incorrect predictions of the CLS for the Si(111)-B surface. In the following section, we use the refined decomposition to analyze the adsorption of CoPc, a large organic molecule.

B. Application of the refined Si 2*p* decomposition: Cobalt phthalocyanine on Si(111)-B

In order to further test the validity of the refined decomposition of Si 2*p* spectra of Si(111)-B, we provide a

comprehensive analysis of its changes upon the adsorption of CoPc on the surface.

In a recent study performed by some of the present authors [6] it was reported that CoPc molecules, deposited at low coverages, lie flat on the surface with the p_z orbital of a Si surface adatom forming a hybrid state with the d_{z^2} orbital of Co. The STM profile of the molecules indicated that the molecular long axis (LA) of CoPc is rotated with respect to the $\langle 110 \rangle$ direction of the surface by about 15°. In this paper as well as in other works [4,7,47], it is reported that a charge transfer from the molecule to the surface takes place.

The Si $2p$ core-level spectra of the clean Si(111)-B surface and for a CoPc surface coverage of 20% (both recorded at a photon energy of 130 eV) are presented in Ref. [6]. It is reported there that after deposition of CoPc at the mentioned coverage a clear change in the Gaussian widths for peaks P2 and P3 is observed, and the intensity of the depth of the valleys between these peaks has decreased. Apart from these changes, all peaks P1–P3 are reported to be shifted by about 0.1 eV to lower binding energies. This change was assigned by the authors to a change in band bending. However, in light of the new decomposition of the Si $2p$ spectrum, this interpretation is revisited in terms of chemical shifts.

In order to model the adsorption of CoPc on Si(111)-B assuming a surface coverage of 20% (i.e., as reported in Ref. [6]), we use $4\sqrt{3} \times 4\sqrt{3}$ surface supercells. This corresponds to a surface coverage with CoPc molecules of 20–25% [see Fig. 3(a)]. Previous STM and DFT studies established that the molecules adsorb in a flat-lying geometry with the central Co atoms atop Si adatoms of the Si(111)-B surface at the investigated submonolayer coverages [4,6,7]. In order to confirm this premise, a large variety of different adsorption sites including the Co atom on top, bridge, hcp-, and fcc-hollow registries have been tested. We also considered the azimuthal orientation of the molecular LA with respect to the surface symmetry $\langle 110 \rangle$ axis as a reference for molecular orientations (ϕ). The value of ϕ is varied between 0 and 15° (note that the cases $\phi = 0°$ and $\phi = 30°$ are equivalent) and the corresponding adsorption energies are calculated.

In a clear agreement with the experiment, the calculations show that the most stable structure is where the Co atom of CoPc adsorbs on top of a Si adatom from the surface [Fig. 3(a)]. The molecular LA is azimuthally oriented by 15° with respect to the high-symmetry axis of the surface (for $\phi = 0°$, the structure is less stable by 150 meV). The adsorption energy of the most stable structure is calculated to be -2.43 eV with a vdW contribution of about 77%. Upon adsorption of CoPc on Si(111)-B, the Si adatom, on which the molecule anchors (of S3 type) is shifted upwards by $d_1 = 0.021$ nm. The Si atom in the third layer beneath the B atom (of S2 type) is shifted by $d_2 = 0.005$ nm downwards. Apart from this, small shifts in the range of 0.001–0.002 nm take place for other surface atoms beneath CoPc. Judging from the reported charge transfer to the substrate, core-level shifts to lower BE are expected, at least, for Si atoms being perturbed by CoPc adsorption. One should note here that the perturbed Si atoms can be categorized in two ways: The first is related to Si atoms, which are strongly perturbed as a result of the bond formation [highlighted in dark gray in Fig. 3(b)]. The second is related to Si atoms beneath the CoPc molecule but

just weakly perturbed [highlighted in light gray in Fig. 3(b)]. Apart from the perturbed Si atoms, there are regions of the surface remaining uncovered during the molecular deposition at the studied submonolayer coverages (unperturbed surface regions). In order to distinguish these regions from each other, we denote them in the following as S, W, and U, respectively.

Figures 3(c)–3(g) show the detailed changes of each surface component upon adsorption of a CoPc molecule in a $4\sqrt{3} \times 4\sqrt{3}$ cell. Note that the surface layer (three atomic layers) in a $4\sqrt{3} \times 4\sqrt{3}$ unit cell contains 144 Si atoms, which are now distributed within the S, W, and U categories. Being relatively uninvolved in the bond formation, the Si atoms of the S1 component have been barely affected: The changes are restricted to shifts less than 0.1 eV of the W category. The S:W:U ratio is 0:6:26 [see Fig. 3(c)]. However, the S2 component behaves differently compared to S1. Upon adsorption of CoPc, the BE of the Si atom in the third layer vertically beneath the B atom is shifted to lower BE by 0.6 eV (strongly perturbed). The BE of the W category is also shifted to lower BE by about 0.15 eV. The S:W:U ratio is 1:4:11 [see Fig. 3(d)]. Figures 3(e) and 3(f) show the changes in the S3 and S4 components upon CoPc adsorption. These changes are comparable to those of S2. Thus, the S:W:U ratios are 1:6:9 and 3:10:35, respectively. The S and W components are shifted by 0.4 and 0.1 eV, respectively, with respect to U. Similar to S1, the component S5 is barely influenced by the CoPc adsorption. Only the BE of the atoms beneath the CoPc molecule have been shifted by about 0.15–0.2 eV to lower BE. The S:W:U ratio is 0:6:26 [see Fig. 3(g)].

Figure 3(h) combines the contributions of all Si types and explains the changes in the Si $2p$ core level upon CoPc adsorption. The total spectrum shown as a black solid line in Fig. 3(h) exhibits a four-peak structure. It can be fitted now by three different three-peak components: (1) A structure contributing 74% that results from the uncovered surface regions. (2) A second structure contributing 22.5%, shifted by about 0.1 eV to lower BE that results from Si atoms weakly perturbed by CoPc adsorption. The latter component is, thus, mainly responsible for the observed changes in the Si $2p$ spectra upon CoPc adsorption observed in Ref. [6]. (3) A component contributing 3.5% shifted by about 0.4 eV to lower BE. This component is related to the Si atoms that are strongly affected by the bond formation, thus, yielding a fourth small peak (P1*). However, the intensity of the latter peak, which originates from the $p_{3/2}$ structure of the strongly perturbed component of S2, is quite small explaining why it is not observed in the experimental spectra shown in Ref. [6].

Figure 4(a) generalizes the case of the 20% CoPc surface coverage, whereby theoretical Si $2p$ spectra for a variety of CoPc coverages (i.e., different amounts of the uncovered surface) have been generated starting from the result shown in Fig. 3(h). The resulting spectra can be nicely compared with experimental Si $2p$ spectra for a series of CoPc coverages between 10% and 50% [Figures 4(b)–4(d)], measured with photon energies of (b) $h\nu = 130$ eV, (c) $h\nu = 160$ eV, and (d) $h\nu = 200$ eV. As already observed for the clean surface, the intensity of peak P1 increases with increasing photon energy as the measurement probes more bulk Si atoms. As no bulk component is included in the theory spectrum shown in Fig. 4(a), this effect is not visible here. Apart from this,
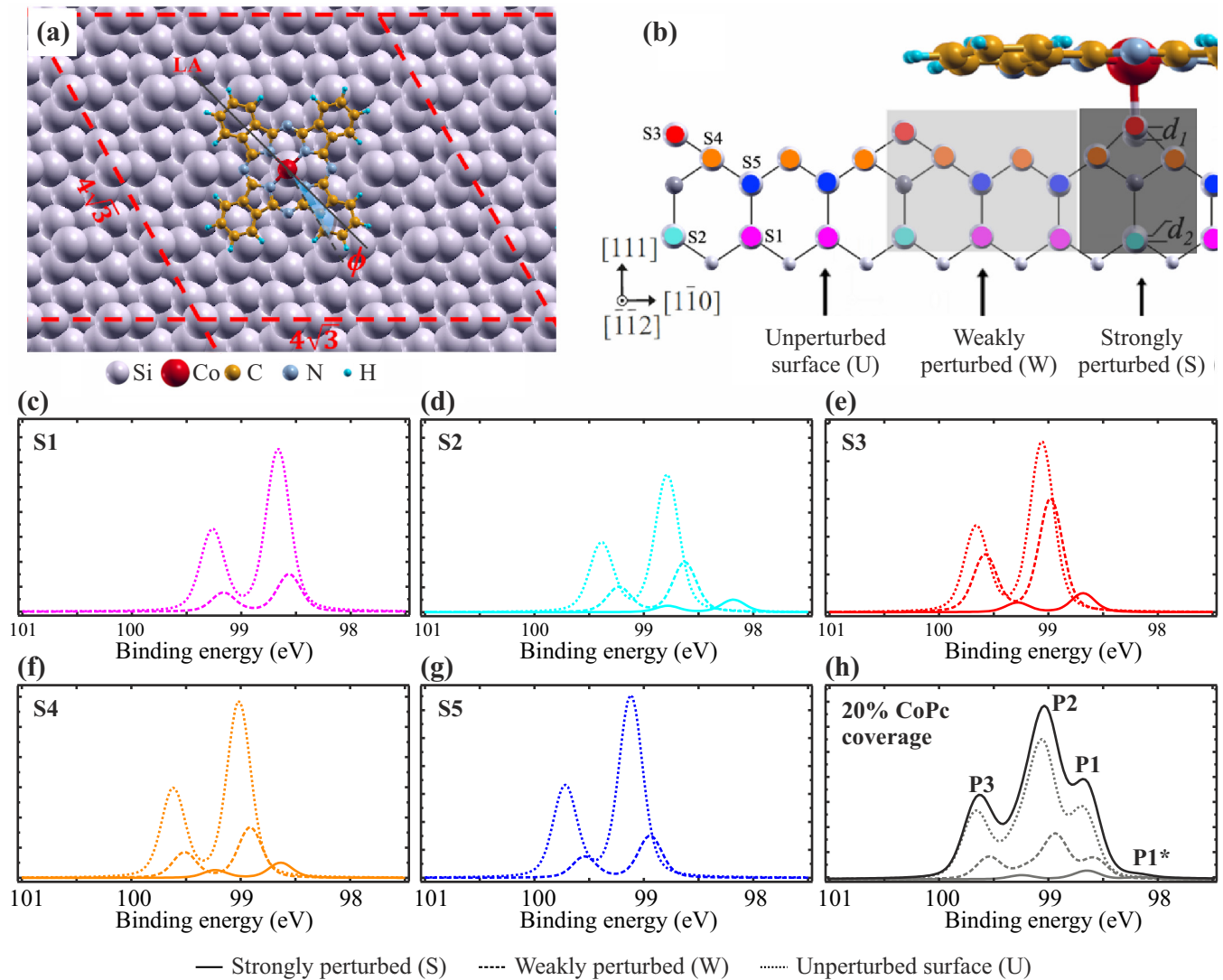
FIG. 3. (a) DFT modeling of an ideal 20% CoPc submonolayer coverage on Si(111)-B in the most stable structure. Surface supercells of dimensions $4\sqrt{3} \times 4\sqrt{3}$ were used. The azimuthal orientation of the molecular LA with respect to the $\langle 110 \rangle$ direction of the surface is denoted as ϕ. (b) Schematic sideview of CoPc adsorbed on the Si(111)-B surface, showing the surface regions, which are differently perturbed by the molecule adsorption. Underneath the central Co where the molecule anchors to the Si adatom, the interaction is strongest. Thereby, the adatom is shifted upwards by d_1, whereas the Si atom in the third layer underneath the B atom is shifted downwards by d_2 (note the original positions given in lighter colors). There are other Si atoms underneath the molecule but weakly perturbed by the CoPc adsorption (W). At the considered low submonolayer coverages, areas of unperturbed surface also still exist. This region is denoted as U. (c)–(g) Separate spectra for the five Si $2p$ surface components, each including proportions of strongly perturbed, weakly perturbed, and unperturbed surface regions. (h) Calculated Si $2p$ spectrum for a 20% surface coverage with CoPc, obtained by adding the components for the different regions.

the agreement between the calculated and the experimental spectra is very good. Upon increasing the coverage of CoPc, a clear tendency of shifts exclusively to lower binding energies is observed, peak P2 becomes broader, and the depth of the valleys between the peaks decreases until the valleys are almost completely filled in the experimental spectra for 50% CoPc. These results explain that the spectral changes are mostly related to the chemical shifts and not only to changes in band bending as previously assumed [6].

C. Angle-resolved photoemission spectroscopy

The valence-band electronic structure of the Si(111)-B surface was investigated using ARPES and interpreted using DFT-PBE calculations. As noted above, several ARPES studies have been carried out on this surface [17,19,25–27,42].

Notably, Grehk *et al.* [25] reported both ARPES and k-resolved inverse photoemission spectroscopy measurements. Two overlapping surface states (termed A_3 and A_3') with bandwidths of 0.4 and 0.7 eV were identified along the $\overline{\Gamma}$-$\overline{M}$ ([10$\overline{1}$]) and $\overline{\Gamma}$-$\overline{K}$-$\overline{M}'$ ([11$\overline{2}$]) directions as well as a state (A_4) around the $\overline{\Gamma}'$ point of the second surface Brillouin zone [(SBZ), cf. Fig. 6]. Thus, a surface state splitting at $\overline{\Gamma}$ of about 0.3 eV between A_3 and A_4 was noted. In contrast, Higashiyama *et al.* [26] found only a single state at $\overline{\Gamma}$ and instead observed a splitting of 0.3 eV between states termed S_1 and S_2 at the $\overline{M}$ point when measured along $\overline{\Gamma}$-$\overline{M}$. The
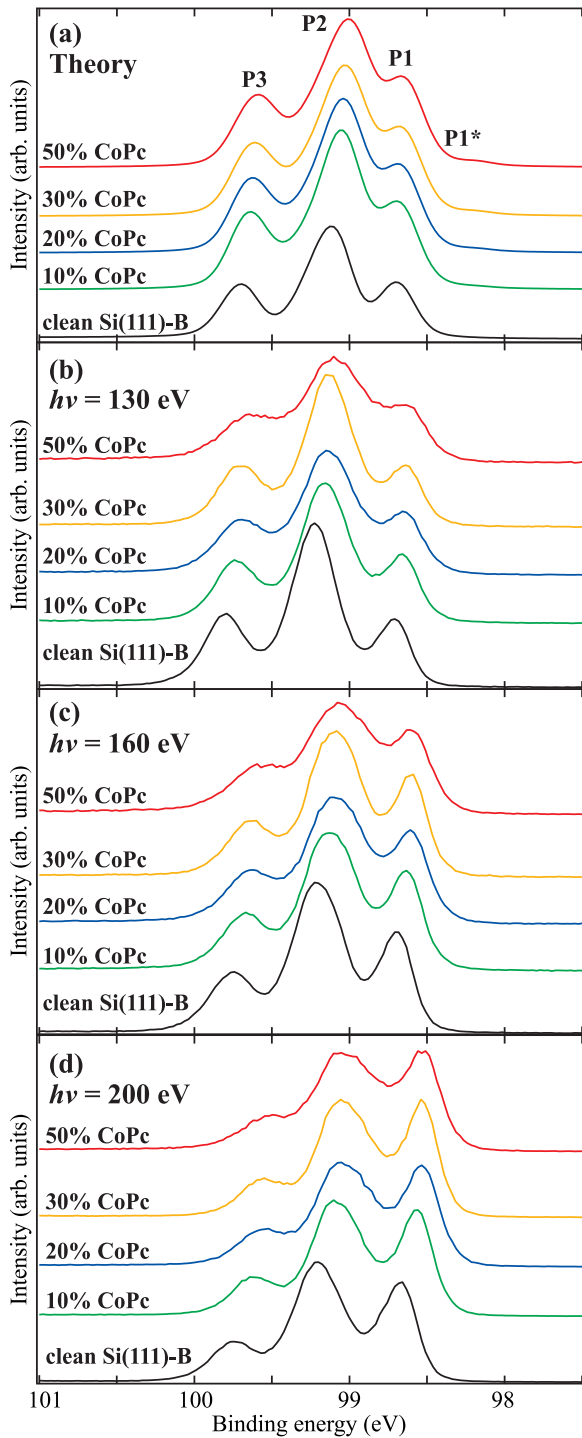
FIG. 4. (a) Generated Si $2p$ spectra assuming different CoPc surface coverages between 10% and 50% and starting from the calculated one for 20%. Here, only the surface components (S1–S5) are considered. The small peak (P1*) originates from the $p_{3/2}$ structure of the atoms in the third layer beneath the B atoms (of S2 type). As a result of anchoring the Co atoms, a charge accumulation between the B atom and the Si atom beneath takes place. As a result, the BE of these Si atoms is shifted to lower values. However, the intensity of peak P1* is too small to be detected experimentally. (b)–(d) Measured changes in Si $2p$ spectra upon increasing the CoPc coverage from 10% to 50% for photon energies of (b) 130, (c) 160, and (d) 200 eV.

bandwidths along $\overline{\Gamma}\text{-}\overline{K}\text{-}\overline{M}'$ and $\overline{\Gamma}\text{-}\overline{M}$ were found to be 0.5 and 0.6 eV. Earlier measurements failed to detect any splitting at these points. These discrepancies among the measured data prompted us to reconsider the valence-band character of Si(111)-B using a more modern ARPES setup in combination with DFT calculations.

The results of the DFT calculations for the valence-band dispersion are shown in Figs. 5(a) and 5(b) for the $\overline{\Gamma}\text{-}\overline{K}\text{-}\overline{M}'$ and the $\overline{\Gamma}\text{-}\overline{M}$ directions, respectively. On the right halves of panels (a) and (b), the k-resolved density of states of the 14-layer Si(111)-B slab, projected onto a surface region (defined here as the top four Si layers plus adatoms, i.e., all atoms shown in Fig. 1) is shown. On the left halves of Figs. 5(a) and 5(b), the band structure of the entire slab is shown. Here, states localized on the adatoms plus their nearest neighbors only (see dashed oval in Fig. 1) are indicated by blue dots, and the projected bulk band structure is shown by gray shaded areas. The calculations succeed to reproduce the previous experimental findings [25,26]. The splitting of two surface states at the $\overline{\Gamma}$ point is nicely reproduced in the calculated band dispersions. The states named A_3 and A_4 by Grehk et $al.$ [25] thereby correspond to the states Γ_1 and Γ_2 in Fig. 5(b). In addition, the splitting at the $\overline{M}$ point observed by Higashiyama et $al.$ [26] is reproduced. However, in our calculations, this splitting is best visible along $\overline{\Gamma}\text{-}\overline{K}\text{-}\overline{M}'$ [cf. states M_1 and M_2 in (a)] whereas Higashiyama et $al.$ observe it mainly along $\overline{\Gamma}\text{-}\overline{M}$. Here, our calculations find four closely spaced bands.

Wave-function plots of these states are shown in Fig. 6. From inspection of states labeled Γ_1, K, and M_2, it is clear that they correspond to a single band spanning the Brillouin zone that is primarily associated with Si-B bonds on the surface plane. Instead, Γ_2 is more localized on Si adatom backbonds and other Si-Si bonds. The upper branch at the $\overline{M}$ point (M_1) is delocalized across several surface layers (not shown). These findings are in general agreement with the calculations of Shi et $al.$ [27].

Figures 5(c)–5(f) show our experimental ARPES results taken along the $\overline{\Gamma}\text{-}\overline{K}\text{-}\overline{M}'$ and $\overline{\Gamma}\text{-}\overline{M}$ directions at a photon energy of 62 eV. The derived band dispersions are presented in Figs. 5(c) and 5(d) as photoemission intensity plots, whereas Figs. 5(e) and 5(f) show them as spectra. Several strongly dispersing bands are seen having a maximum at the valence-band edge at $\overline{\Gamma}$ and a minimum at $\overline{\Gamma}'$ (i.e., $\overline{K}_{1\times1}$) and are, thus, attributed to signals from the bulk (see also the discussion below). Several weakly dispersing intense features are observed with maxima around the $\overline{K}$ and $\overline{M}$ points, which we attribute to the aforementioned surface states. Along the $\overline{\Gamma}\text{-}\overline{K}\text{-}\overline{M}'$ direction [Figs. 5(c) and 5(e)], a surface-state band that disperses upwards from $\overline{\Gamma}$ to $\overline{K}'$ is found with a maximum at $\overline{K}$ at $\sim$0.7 eV below the valence-band maximum (VBM), consistent with the A_3' surface state observed by Grehk et $al.$ [25] and the S_2 surface state observed by Higashiyama et $al.$ [26]. Between $\overline{K}'$ and $\overline{M}'$, this surface-state band splits into two states, one with downward dispersion towards $\overline{M}'$ and one with upward dispersion. This is best visible in Fig. 5(e) where it appears as a shoulder (indicated by dashed lines). Unfortunately, the $\overline{M}'$ point is not completely reached in our measurement, but a splitting of $\sim$0.4 eV is found at the right edge of Fig. 5(e) between the states named M_1 and M_2.
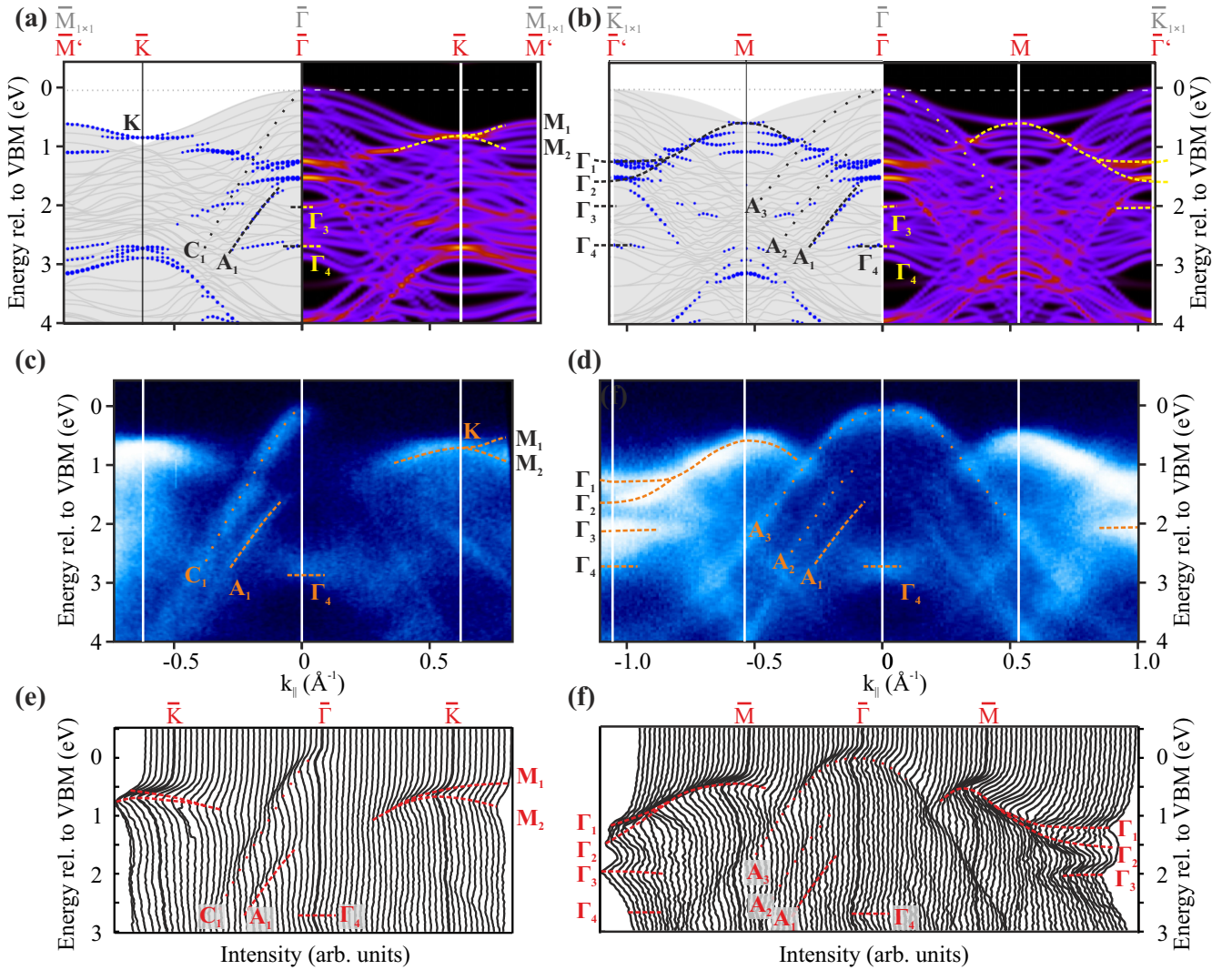
FIG. 5. Band dispersion for the $\overline{\Gamma}$-$\overline{K}$-$\overline{M}'$ and $\overline{\Gamma}$-$\overline{M}$ directions. (a) and (b) The left halves of each panel show the calculated band structures of Si(111)-B. Gray shaded areas indicate the bulk-projected bands. Blue dots indicate states localized on atoms nearest to the adatoms as indicated by the dashed ellipse in Fig. 1. The right halves show the k-resolved density of states projected on atoms in the surface region (defined here as the top four Si layers plus adatoms). (c)–(f) Experimental ARPES data taken with a photon energy of 62 eV as (c) and (d) intensity plots of the dispersion and (e) and (f) as spectra taken at individual $k_\parallel$ values. In the plots, surface and bulk related features are indicated by dashed and dotted lines, respectively. High-symmetry points of the $\sqrt{3} \times \sqrt{3}$ (1×1) cell are indicated in red (gray) (cf. Fig. 6).

Thus, M_1 corresponds to the A_3 (S_1) state found by Grehk *et al.* [25] (Higashiyama *et al.* [26]), whereas M_2 corresponds to A_3' (S_2). Our value of 0.4 eV is in good agreement with Refs. [25,26] as well as our calculations. Although Higashiyama *et al.* observe the splitting predominantly along the $\overline{\Gamma}$-$\overline{M}$ direction, we resolve it better along $\overline{\Gamma}$-$\overline{K}$-$\overline{M}'$. At the $\overline{M}$ point along $\overline{\Gamma}$-$\overline{M}$ [see Figs. 5(d) and 5(f)], we observe a broad and intense feature with maximum at $\overline{M}$, similar to Grehk *et al.* [25]. As mentioned above, this can be related to the presence of four bands in close distance that cannot be resolved individually.

As also found by Grehk *et al.* [25], the intensity of the surface features is weak in the center of the first SBZ, but increases for higher $k_\parallel$ values. Thus, the features at the $\overline{\Gamma}$ point are better visible at $\overline{\Gamma}'$ in Figs. 5(d) and 5(f). As indicated again by dashed lines, we clearly observe a splitting into two bands here. These states, which we call Γ_1 and

Γ_2, correspond to the A_3 and A_4 states in Ref. [25]. Also the observed splitting of ~0.3 eV is in agreement with the calculations as well as with Ref. [25]. Thus, our experiments and calculations clearly succeed in reproducing all surface-related signals of the Si(111)-B surface found in previous studies [25,26].

Furthermore, we observe several additional features, which we can assign to the Si(111)-B surface. These states are again indicated by dashed lines in Fig. 5 whereas bulk signals are indicated by dotted lines. To distinguish between surface- and bulk-related features, we investigate the localization of the states using DFT. In doing so, we could identify two features Γ_3 and Γ_4 located around the $\overline{\Gamma}$ point at ~2.0 and ~2.7 eV below the VBM, respectively. Inspection of their wave-function character (Fig. 6) reveals that they are highly localized and arise from downward backbonds of Si (Γ_3) or B (Γ_4) atoms of the second atomic layer.
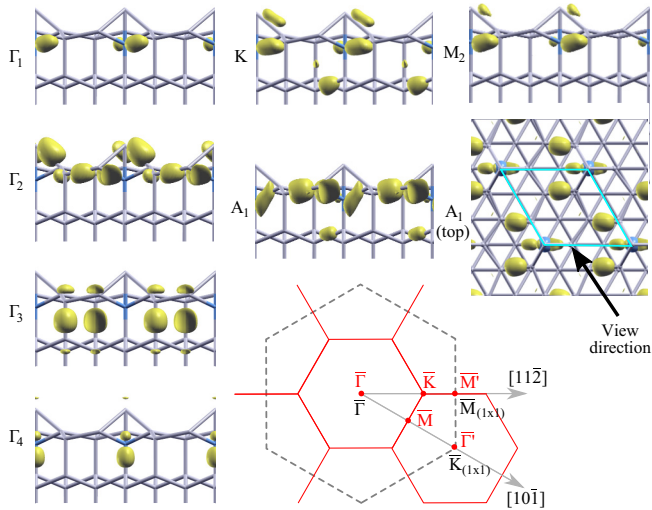
FIG. 6. Wave functions of selected states via isosurface plots of $|\psi|^2$ (at 1/3 of their maximum value). The character of A_1 is quite independent of k. The SBZ is also shown.

Next, we turn our attention on the highly dispersive bands around $\overline{\Gamma}$. One of these bands (A_1) is also found in the surface localized states shown in Figs. 5(a) and 5(b). According to the wave-function plots in Fig. 6, A_1 derives from Si-Si bonds of the top two Si atomic layers. These are spread across the entire surface unit cell (see top view), which explains the strong dispersion of the band in both directions studied. In contrast, the bands A_2, A_3, and C_1 are bulk related.

The symmetry of the various surface states is revealed in the constant energy slices displayed in Fig. 7. The left- (right-) hand side shows the experimental (theoretical) results. The experimental data are nicely reproduced in the calculations. Plots for an energy of 0.5 eV below the VBM are shown in (a). High intensity regions appear at the $\overline{M}$ points of the $\sqrt{3} \times \sqrt{3}$ SBZ in both experimental and theoretical data, corresponding to the maxima of the weakly dispersion surface-state band (see Fig. 5). At 0.7 eV below the VBM [Fig. 7(b)], the band is cut at the $\overline{M}$ points leading to the observation of elliptical features around the $\overline{M}$ points. A higher intensity is visible at the $\overline{K}$ points where the band exhibits a saddle point (labeled K in Fig. 5). At 1.0 eV below the VBM [Fig. 7(c)], the calculations reveal a hexagon within the first $\sqrt{3} \times \sqrt{3}$ SBZ, which leads to dumbbell-like features in the second SBZ. Due to the weak intensity within the first SBZ (as mentioned above), the hexagon in the center is only faintly visible in the experiment, whereas the dumbbell features in the second SBZ are better reproduced. The plots in Fig. 7(d) for an energy of 1.4 eV below the VBM show the distribution of the Γ_1 and Γ_2 surface states appearing as relatively broad rings at the $\overline{\Gamma}$ points. Again, due to the weak intensity in the first SBZ, they are better visible in the second SBZ around the $\overline{\Gamma}'$ points. In Fig. 7(e), the constant energy cut for 2.0 eV below the VBM is shown, corresponding to the energy of the Γ_3 state. In both experimental and theoretical plots, ringlike features are visible around the $\overline{\Gamma}$ points. The inner ring is thereby assigned to the Γ_3 state, whereas the second ring (in the experimental plot best visible in the first SBZ) is assigned to the A_1 band that
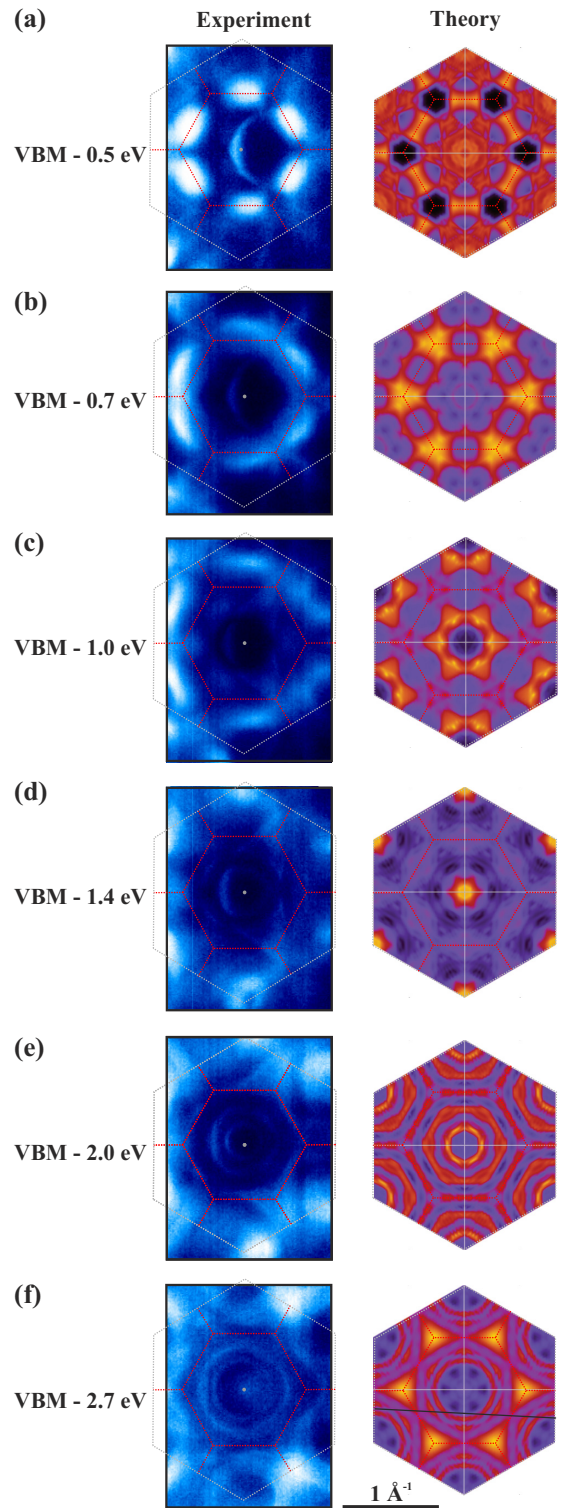
FIG. 7. Constant energy slices through the whole surface Brillouin zone. Left: experimental data. Right: k-resolved DOS, projected on atoms in the surface region. The SBZ of the $\sqrt{3} \times \sqrt{3}$ and 1×1 cells are shown in red and gray, respectively.

cuts the energy surface. For an energy of 2.7 eV below the VBM, i.e., the energetic position of the Γ_4 state [see Fig. 7(f)], we again observe ringlike features around the $\overline{\Gamma}$ points, which are now assigned to the Γ_4 states.

IV. CONCLUSIONS

Our combined approach of core-level and angle-resolved photoemission spectroscopy as well as DFT simulations provides an insight into the electronic structure of the Si(111)-B surface and revises previous unsatisfactory attempts to understand the Si $2p$ photoemission spectra and valence-band electronic structure. Importantly, the decomposition of the Si $2p$ spectra into the maximum possible six components surpass all previous investigations available. The theory-guided fits contain five surface components (S1–S5), which we assign to the following structural regions: The S2 (S1) component corresponds to the $\frac{1}{3}$ ML ($\frac{2}{3}$ ML) of Si in the third layer binding (not binding) to B. The S3 component arises from $\frac{1}{3}$ ML of Si adatoms, whereas S4 stems from 1 ML of Si atoms in the first layer. The S5 component arises from $\frac{2}{3}$ ML of Si atoms in the second layer not binding to B. The S1–S5 components are shifted with respect to the bulk Si by about 0.05, 0.15, 0.40, 0.50, and 0.60 eV, respectively. While the intensity ratio of these components is fixed, the contribution of the Si bulk depends on the photon energy and is easily identified here. As demonstrated for CoPc submonolayer coverages on Si(111)-B, these results are important for a thorough understanding of molecular and atomic adsorption on this surface. Furthermore, our combined DFT and ARPES investigations reveal a comprehensive picture of the electronic structure of the valence band. We are able to clarify known surface states as well as to identify a number of unknown localized and dispersive surface states. Finally, on the basis of constant energy plots of the photoemission intensity, we mapped their distribution in $k_\parallel$ space.

To summarize, the present paper provides a cornerstone for a comprehensive characterization of the electronic structure of the Si(111)-B surface. The new decomposition of the Si $2p$ core level, not accessible with the experiment, provides a basis for future interpretations of molecular self-assembly on this important template substrate.

[1] Y. Makoudi, F. Palmino, E. Duverger, M. Arab, F. Chérioux, C. Ramseyer, B. Therrien, M. J.-L. Tschan, and G. Süss-Fink, Nondestructive Room-Temperature Adsorption of 2, 4, 6-tri(2′-thienyl)−1, 3, 5-triazine on a Si-B Interface: High-Resolution STM Imaging and Molecular Modeling, Phys. Rev. Lett. **100**, 076405 (2008).

[2] B. Baris, V. Luzet, E. Duverger, P. Sonnet, F. Palmino, and F. Cherioux, Robust and open tailored supramolecular networks controlled by the template effect of a silicon surface, Angew. Chem., Int. Ed. **50**, 4094 (2011).

[3] S. R. Wagner, R. R. Lunt, and P. Zhang, Anisotropic Crystalline Organic Step-Flow Growth on Deactivated Si Surfaces, Phys. Rev. Lett. **110**, 086107 (2013).

[4] S. R. Wagner, B. Huang, C. Park, J. Feng, M. Yoon, and P. Zhang, Growth of Metal Phthalocyanine on Deactivated Semiconducting Surfaces Steered by Selective Orbital Coupling, Phys. Rev. Lett. **115**, 096101 (2015).

[5] Y. Makoudi, J. Jeannoutot, F. Palmino, F. Cherioux, G. Copie, C. Krzeminski, F. Cleri, and B. Grandidier, Supramolecular self-assembly on the B-Si(111)-($\sqrt{3} \times \sqrt{3}$) R30° surface: From single molecules to multicomponent networks, Surf. Sci. Rep. **72**, 316 (2017).

[6] S. Lindner, M. Franz, M. Kubicki, S. Appelfeller, M. Dähne, and H. Eisele, Arrangement and electronic properties of cobalt phthalocyanine molecules on B-Si(111)-$\sqrt{3} \times \sqrt{3}$ R30°-B, Phys. Rev. B **100**, 245301 (2019).

[7] M. Kubicki, S. Lindner, M. Franz, H. Eisele, and M. Dähne, Adsorption behavior of cobalt phthalocyanine submonolayer coverages on Si $\sqrt{3} \times \sqrt{3}$R30°-B, J. Vac. Sci.Technol. B **38**, 042803 (2020).

[8] H. Hirayama, T. Tatsumi, and N. Aizaki, Reflection high energy electron diffraction and Auger electron spectroscopic study on B/Si(111) surfaces, Surf. Sci. **193**, L47 (1988).

[9] V. V. Korobtsov, V. G. Lifshits, and A. V. Zotov, Formation of Si(111)$\sqrt{3} \times \sqrt{3}$-B and Si epitaxy on Si(111)$\sqrt{3} \times \sqrt{3}$-B: LEED-AES study, Surf. Sci. **195**, 466 (1988).

[10] R. L. Headrick, I. K. Robinson, E. Vlieg, and L. C. Feldman, Structure Determination of the Si(111):B($\sqrt{3} \times \sqrt{3}$)R30° Surface: Subsurface Substitutional Doping, Phys. Rev. Lett. **63**, 1253 (1989).

[11] P. Bedrossian, R. D. Meade, K. Mortensen, D. M. Chen, J. A. Golovchenko, and D. Vanderbilt, Surface Doping and Stabilization of Si(111) with Boron, Phys. Rev. Lett. **63**, 1257 (1989).

[12] I.-W. Lyo, E. Kaxiras, and P. Avouris, Adsorption of Boron on Si(111): Its Effect on Surface Electronic States and Reconstruction, Phys. Rev. Lett. **63**, 1261 (1989).

[13] H. Huang, S. Y. Tong, J. Quinn, and F. Jona, Atomic structure of Si(111) ($\sqrt{3} \times \sqrt{3}$R30°)-B by dynamical low-energy electron diffraction, Phys. Rev. B **41**, 3276 (1990).

[14] P. Baumgärtel, J. J. Paggel, M. Hasselblatt, K. Horn, V. Fernandez, O. Schaff, J. H. Weaver, A. M. Bradshaw, D. P. Woodruff, E. Rotenberg *et al.*, Structure determination of the ($\sqrt{3} \times \sqrt{3}$)R30° boron phase on the Si(111) surface using photoelectron diffraction, Phys. Rev. B **59**, 13014 (1999).

[15] A. B. McLean, L. J. Terminello, and F. J. Himpsel, Electronic structure of Si(111)-B($\sqrt{3} \times \sqrt{3}$)R30° studied by Si $2p$ and B 1s core-level photoelectron spectroscopy, Phys. Rev. B **41**, 7694 (1990).

[16] Y. Ma, J. E. Rowe, E. E. Chaban, C. T. Chen, R. L. Headrick, G. M. Meigs, S. Modesti, and F. Sette, Surface

States and Alkali-to-Semiconductor Charge Transfer in the K/Si(111)($\sqrt{3} \times \sqrt{3}$)R(30°)-B System, Phys. Rev. Lett. **65**, 2173 (1990).

[17] E. Kaxiras, K. C. Pandey, F. J. Himpsel, and R. M. Tromp, Electronic states due to surface doping: Si(111)$\sqrt{3} \times \sqrt{3}$B, Phys. Rev. B **41**, 1262 (1990).

[18] J. E. Rowe, G. K. Wertheim, and D. M. Riffe, Silicon (2p) surface core-leve line shape of Si(111)-B, J. Vac. Sci. Technol. A **9**, 1020 (1991).

[19] H. H. Weitering, J. Chen, N. J. DiNardo, and E. W. Plummer, Electron correlation, metallization, and Fermi- level pinning at ultrathin K/Si(111) interfaces, Phys. Rev. B **48**, 8119 (1993).

[20] T. M. Grehk, M. Göthelid, U. O. Karlsson, L. S. O. Johansson, S. M. Gray, and K. O. Magnusson, Clean and Cs-exposed Si(111)$\sqrt{3} \times \sqrt{3}$:B surface studied with high-resolution photoemission, Phys. Rev. B **52**, 11165 (1995).

[21] J. Krügener, H. J. Osten, and A. Fissel, Ultraviolet photoelectron spectroscopic study of boron adsorption and surface segregation on Si(111), Phys. Rev. B **83**, 205303 (2011).

[22] Y. Fagot-Revurat, C. Tournier-Colletta, L. Chaput, A. Tejeda, L. Cardenas, B. Kierren, D. Malterre, P. L. Fèvre, F. Bertran, and A. Taleb-Ibrahimi, Understanding the insulating nature of alkali-metal/Si(111):B interfaces, J. Phys.: Condens. Matter **25**, 094004 (2013).

[23] S. Menzli, A. Laribi, H. Mrezguia, I. Arbi, A. Akremi, C. Chefi, F. Chérioux, and F. Palmino, Photoelectron spectroscopic studies of ultra-thin CuPc layers on a Si(111)-($\sqrt{3} \times \sqrt{3}$)R30°-B surface, Surf. Sci. **654**, 39 (2016).

[24] Here, the measurement takes place near the minimum of the universal curve (mean free electron path) [46], being, thus, very surface sensitive (see Ref. [15]).

[25] T. M. Grehk, P. Mårtensson, and J. M. Nicholls, Occupied and unoccupied surface states on the Si(111)$\sqrt{3} \times \sqrt{3}$:B surface, Phys. Rev. B **46**, 2357 (1992).

[26] K. Higashiyama and S. Yamazaki and H. Ohnuki and H. Fukutani, Surface states of boron-induced $\sqrt{3} \times \sqrt{3}$ structure on Si(1 1 1), Solid State Commun. **87**, 455 (1993).

[27] H. Q. Shi, M. W. Radny, and P. V. Smith, Electronic structure of the Si(111) $\sqrt{3} \times \sqrt{3}$R30° -B surface, Phys. Rev. B **66**, 085329 (2002).

[28] P. Giannozzi, S. Baroni, N. Bonini, M. Calandra, R. Car, C. Cavazzoni, D. Ceresoli, G. L. Chiarotti, M. Cococcioni, I. Dabo *et al.*, QUANTUM ESPRESSO: A modular and open-source software project for quantum simulations of materials, J. Phys.: Condens. Matter **21**, 395502 (2009).

[29] J. P. Perdew, K. Burke, and M. Ernzerhof, Generalized Gradient Approximation Made Simple, Phys. Rev. Lett. **77**, 3865 (1996).

[30] S. Grimme, J. Antony, S. Ehrlich, and H. Krieg, A con- sistent and accurate ab initio parametrization of density functional dispersion correction (DFT-D) for the 94 elements H-Pu, J. Chem. Phys. **132**, 154104 (2010).

[31] F. Ortmann, F. Bechstedt, and W. G. Schmidt, Semiempirical van der Waals correction to the density functional description of solids and molecular structures, Phys. Rev. B **73**, 205101 (2006).

[32] D. M. Ceperley and B. J. Alder, Ground State of the Electron Gas by a Stochastic Method, Phys. Rev. Lett. **45**, 566 (1980).

[33] E. Pehlke and M. Scheffler, Evidence for Site-Sensitive Screening of Core Holes at the Si and Ge (001) Surface, Phys. Rev. Lett. **71**, 2338 (1993).

[34] W. G. Schmidt, P. Käckell, and F. Bechstedt, 3d core-level shifts at SeGaAs(110), Surf. Sci. **357-358**, 545 (1996).

[35] S. García-Gil, A. García, and P. Ordejón, Calculation of core level shifts within DFT using pseudopotentials and localized basis sets, Eur. Phys. J. B **85**, 239 (2012).

[36] H. Aldahhak, M. Paszkiewicz, F. Allegretti, D. A. Duncan, S. Tebi, P. S. Deimel, P. A. Casado, Y.-Q. Zhang, A. C. Papageorgiou, R. Koch *et al.*, X-ray spectroscopy of thin film free-base corroles: A combined theoretical and experimental characterization, J. Phys. Chem. C **121**, 2192 (2017).

[37] H. Aldahhak, M. Paszkiewicz, E. Rauls, F. Allegretti, S. Tebi, A. C. Papageorgiou, Y.-Q. Zhang, L. Zhang, T. Lin, T. Paintner *et al.*, Identifying on-surface site-selective chemical conversions by theory-aided NEXAFS spectroscopy: The case of free-base corroles on Ag(111), Chem. Eur. J. **24**, 6787 (2018).

[38] S. Tebi, M. Paszkiewicz, H. Aldahhak, F. Allegretti, S. Gonglach, M. Haas, M. Waser, P. S. Deimel, P. C. Aguilar, Y.-Q. Zhang *et al.*, On-surface site-selective cyclization of corrole radicals ACS Nano **11**, 3383 (2017).

[39] H. Aldahhak, P. Powroźnik, P. Pander, W. Jakubik, F. B. Dias, W. G. Schmidt, U. Gerstmann, and M. Krzywiecki, Toward efficient toxic-gas detectors: Exploring molecular interactions of sarin and dimethyl methylphosphonate with metal-centered phthalocyanine structures, J. Phys. Chem. C **124**, 6090 (2020).

[40] M. Paszkiewicz, T. Biktagirov, H. Aldahhak, F. Allegretti, E. Rauls, W. Schöfberger, W. G. Schmidt, J. V. Barth, U. Gerstmann, and F. Klappenberger, Unraveling the oxidation and spin state of Mn-corrole through x-ray spectroscopy and quantum chemical analysis, J. Phys. Chem. Lett. **9**, 6412 (2018).

[41] P. E. Blöchl, Phys. Rev. B **50**, 17953 (1994).

[42] R. Cao, X. Yang, and P. Pianetta, Characterization of the B/Si surface electronic structures, J. Vac. Sci.Technol. A **11**, 1817 (1993).

[43] S. A. Khan, M. Vondráček, P. Blaha, K. Horáková, J. Minár, O. Šipr and V. Cháb, Local geometry around B atoms in B/Si(111) from polarized x-ray absorption spectroscopy, J. Phys.: Condens. Matter **32**, 045901 (2019).

[44] J. Chang and M. J. Stott, Si(111)/B surface reconstruction and related phenomena, Phys. Status Solidi B **200**, 481 (1997).

[45] In the so-called T_4 model, the deposited atoms (e.g., Al, Ga, and In) reside on the fourfold coordinated adatom site directly above atoms in the the second sublayer and forming three bonds with atoms in the first layer. A good description of the different adsorption sites can be found in Ref. [48].

[46] M. P. Seah and W. A. Dench, Quantitative electron spectroscopy of surfaces: A standard data base for electron inelastic mean free paths in solids, Surf. Interface Anal. **1**, 2 (1979).

[47] R. G. A. Veiga, R. H. Miwa, and A. B. McLean, Adsorption of metal-phthalocyanine molecules onto the Si(111) surface passivated by δ doping: Ab initio calculations, Phys. Rev. B **93**, 115301 (2016).

[48] F. Bechstedt, *Principles of Surface Physics* (Springer, Berlin, Heidelberg, 2003).